AUTOMATIC SEGMENTATION OF LUNG LOBES IN CT IMAGES BASED ON FISSURES, VESSELS, AND BRONCHI

Bianca Lassen, Jan-Martin Kuhnigk, Ola Friman, Stefan Krass, Heinz-Otto Peitgen

Fraunhofer MEVIS – Institute for Medical Image Computing, Bremen, Germany

ABSTRACT

Lobewise analysis of the pulmonary parenchyma is of clinical relevance for diagnosing and monitoring pathologies. In this work, a fully automatic lobe segmentation approach is presented, which is based on a previously proposed watershed transformation approach. The proposed extension explicitly considers the pulmonary fissures by including them in the cost image for the watershed segmentation. The fissure structures are found through a tailored feature analysis of the Hessian matrix. The method is evaluated using 42 data sets, and a comparison with manual segmentations yields an average volumetric agreement of 96.8%. In comparison to the previously proposed approach, this method increases segmentation accuracy where the fissures are visible.

***Index Terms*—** lung lobes, pulmonary fissures, segmentation

1. INTRODUCTION

The human lungs are subdivided into distinct pulmonary lobes separated by thin barriers, called fissures (Fig 1a). The right lung consists of an upper, middle, and lower lobe, whereas the left lung consists of only an upper and a lower lobe. Each lobe contains separate supply branches for both vessels and airways. Segmentation of the pulmonary lobes is relevant in many clinical applications. For example, lobewise quantification of pulmonary parenchyma is useful for diagnosing and monitoring pathologies such as emphysema or fibrosis. Some diseases, such as lung cancer, limited to a single lobe, require resection of a single lobe. In these cases, lung lobe segmentation can support pre-operative planning by providing information about the residual functional parenchyma. Pulmonary lobe segmentation is a challenging task due to the varying image resolution and quality obtained with different CT scanners and acquisition protocols. Moreover, variations in anatomy are frequent, and incomplete fissures are common, especially in severe lung disease cases (Fig.1).

Several automatic and semi-automatic lobe segmentation methods have been proposed in the literature. Rikxoort et al. [1] and Zhang et al. [2] proposed an automatic lobe segmentation based on an anatomic pulmonary atlas. Rikxoort et al. [3] introduced another automatic lobe segmentation approach including a supervised fissure enhancement filter and grouping of adjacent fissure voxels into plates. Kuhnigk et al. [4] and Ukil et al. [5] used a watershed transformation based on a cost image calculated by a distance transform to the vasculature. Ross et al. [6] proposed a semi-automatic lobe segmentation in which fissures are calculated by a thin plate spline method based on markers set interactively on the fissure. Wang et al. [7] applied semi-automatic 2D fissure enhancement and 3D fissure interpolation to segment the lung into lobes.

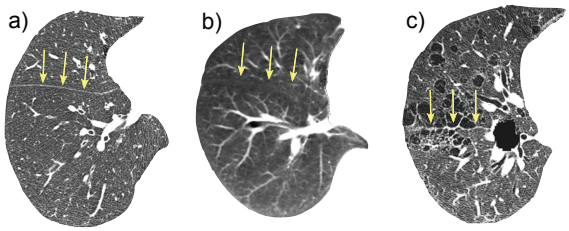

Fig. 1. Three axial CT scans of the right lung from different patients. Arrows point to the lobe boundaries. a) Clear major fissure (0.77 mm x 0.77 mm x 0.8 mm) b) Blurred major fissure caused by low resolution (0.7 mm x 0.7 mm x 5.0 mm) c) Unsharp major fissure caused by emphysema (0.72 mm x 0.72 mm x 1.0 mm).

This paper proposes an extension of a previously published lobe segmentation method [4], which has already been applied to more than 1000 datasets [8]. The previous method is based on the analysis of lobar airways and vasculature, and is therefore relatively robust with respect to incomplete or missing fissures. However, its results are frequently inaccurate, even in the vicinity of clearly visible fissures, and often require manual correction. The new method proposed in this paper complements the previous approach by explicitly segmenting visible fissure fragments and integrating the new information into the well-proven existing segmentation framework.

2. METHODS

The developed lung lobe segmentation method is based on the existing framework MeVisPULMO [4], a research software tool for automatic analysis of lung parenchyma. The tool includes segmentation methods for both lungs, the bronchial

Authorized licensed use limited to: UCLA Library. Downloaded on August 24,2021 at 19:29:47 UTC from IEEE Xplore. Restrictions apply.

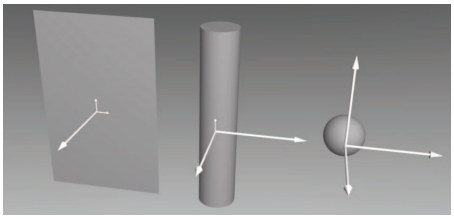

Fig. 2. Eigenvectors of the Hessian matrix for a sheet, a tube, and a blob. A sheet has one large and two small eigenvalues. In contrast, the tube and the blob structures have two or three large eigenvalues.

tree, and the pulmonary vessels, described in detail in [4]. These methods are reused for the proposed extension.

In the lobe segmentation framework, a watershed transformation provides a segmentation of the lung lobes. The markers for the watersheds are automatically generated from the bronchi tree. In the former version, the watershed cost image was based on the vasculature distance and the original CT data. The proposed extension is an explicit consideration of the fissures in the calculation of the watershed cost image. In the following sections, the segmentation of the pulmonary fissures and the calculation of the improved cost image are described in detail. When not otherwise stated, all calculations are carried out voxelwise.

Fissure enhancement

The Hessian matrix $\mathbf{H}$ of an image contains the second-order partial derivatives, and the relation between the eigenvalues $|\lambda_1| \leq |\lambda_2| \leq |\lambda_3|$ of $\mathbf{H}$ describes the local image structure. In this work, $\mathbf{H}$ is calculated using a derivative-of-Gaussian approach with $\sigma = 1.0$ mm. Fissures can locally be modeled as a sheet where the eigenvalue orthogonal to the fissure plane is large, and the other two eigenvalues are small, see Fig. 2. Thus, on the bright fissures, the ideal relationship is $|\lambda_1| = |\lambda_2| = 0$ and $\lambda_3 \ll 0$. Vessels and nodules exhibit strong gradients in more than one direction, i.e., $|\lambda_2| \gg 0$. In addition, these structures exhibit a larger $|\lambda_3|$ compared to fissures because of their stronger image contrast, as seen in Fig. 1. Hence, fissure voxels may be characterized as follows: $0 \ll |\lambda_3| < \delta$ and $|\lambda_2| \approx 0$, where δ describes the average $|\lambda_3|$ value for vessels. Specifically, the following feature functions are introduced (Fig. 3):

$$F_{Structure} = \Theta(-\lambda_3) e^{\frac{-(\lambda_3-\alpha)^6}{\beta^6}} \text{ and } F_{Sheet} = e^{\frac{-\lambda_2^6}{\gamma^6}}. \quad (1)$$

$F_{Structure}$ rates the strength of image structure. Because the intensity of the fissure structure varies both between patients and also within a single data set, a wide interval of intensities for high fissure probability is defined. The following values were found by empirically examining a λ_3-histograms of fissure voxels: $\alpha = 50$, $\beta = 35$ (resulting in $\delta \approx 100$). The term $\Theta(-\lambda_3)$ describes a heaviside function that sets $F_{Structure}$ to 0 for voxels with $\lambda_3 \geq 0$, i.e., a dark structure on a bright

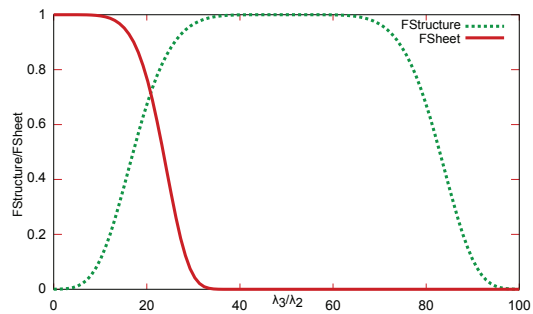

Fig. 3. Plot of $F_{Structure}$ and F_{Sheet}. X-axis refers to λ_3 for $F_{Structure}$ and to λ_2 for F_{Sheet}.

background is not a fissure. The F_{Sheet} feature discriminates between a sheet structure and other structures such as nodules or vessels, as these latter structures have larger $|\lambda_2|$ values. γ is empirically set to 25 by investigating typical values for fissures and other high-contrast structures within the lung. $F_{Structure}$ and F_{Sheet} are in the range $[0, 1]$. The overall fissure similarity measure $S_{Fissure}$ is defined as the product:

$$S_{Fissure} = F_{Structure} F_{Sheet}. \quad (2)$$

Fissure segmentation

The first step of the fissure segmentation is to define a voxel mask C with candidate fissure voxels. The mask is constructed by combining the contrast and structure information in $S_{Fissure}$ with the CT image voxel intensity:

$$C = [S_{Fissure} > 0.1\,] \wedge [I_v < (\mu_{vessel} - 2\sigma_{vessel})], \quad (3)$$

where μ_{vessel} and σ_{vessel} are the mean intensity and standard deviation of vessel voxels, respectively. These parameters are estimated individually for each CT data set. The purpose of the gray value information is to exclude vessels which usually have higher intensities than fissures and are not already excluded by $F_{Structure}$.

Next, a 3D connected component analysis is performed on the candidate voxels in C. The largest eigenvalue of a sheet is perpendicular to the plate. Thus, the corresponding eigenvector of the largest eigenvalue shows the orientation of a structure. The curvature of a fissure is locally very low, so adjacent fissure voxels have similar largest eigenvectors. Taking advantage of this property, a vector-based connected component analysis is applied, similar to Rikxoort et al. [3]. The similarity is calculated by the inner product of the normalized eigenvectors, so that the inner product is 1 for identical vectors. Thus, adjacent voxels inside the ROI with an inner product ≥ 0.98 are joined to a connected component. All components with a volume of at least 0.1 ml (corresponding to 400 voxels for a resolution of x,y = 0.5 mm and z = 1 mm) are kept, and a morphological closing is applied to close minor gaps.

Authorized licensed use limited to: UCLA Library. Downloaded on August 24,2021 at 19:29:47 UTC from IEEE Xplore. Restrictions apply.

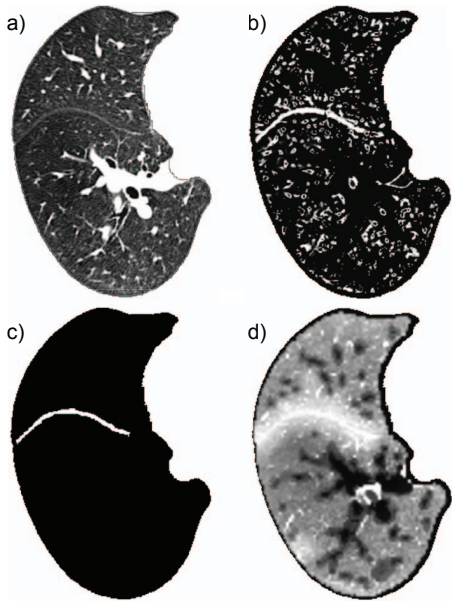

Fig. 4. An axial CT slice of an isolated right lung: a) Original image b) Fissure similarity c) Fissure Segmentation d) Cost image.

Watershed cost image computation

To be able to handle incomplete fissures, the segmentation of the visible fissure parts needs to be complemented with additional information. For segmenting the lobes, a marker-based watershed transform similar to the one in [4] is used. In extension to [4], the cost image calculation for the watershed transformation is based on the vessel tree, the bronchi tree, the pulmonary fissures, and the original image. As each pulmonary lobe has its own bronchi and vessel system, there is usually no major supply branch near the lobe boundaries. Hence, the Euclidean distance transformations d_b and d_v from these trees generally yield large distances at the lobe boundaries. To incorporate fissure information into the cost image only in the regions of well segmented fissure, a ROI of influence is first defined in a distance α around the fissure. In this ROI, a Euclidean distance transformation d from the fissures is calculated. Because the cost image requires high values at the fissures, the result of the distance transformation is inverted, and the square is calculated to additionally emphasize the fissure: $d_f = (\alpha - d)^2, d \leq \alpha$. The anticipated effect of the original image is to enhance fissures that would possibly not be found by the fissure segmentation. All four information sources (d_b, d_v, d_f and the original image) are combined with equal weight to a single cost image. Based on this cost image, the watershed transformation is performed as in the earlier version of the segmentation framework. Figure 4 shows the results of the three processing steps: fissure enhancement, fissure segmentation, and the cost image.

	Experiment 1		Experiment 2			
Lobe	NA	PA	Intra1	Intra2	Inter1	Inter2
LU	98.2	97.4	99.2	98.2	99.3	97.5
LL	97.9	97.0	99.0	98.9	99.1	98.4
RU	97.1	96.6	98.8	97.1	99.0	94.7
RM	92.8	90.2	96.9	96.4	97.6	96.2
RL	97.9	97.1	98.6	98.0	99.0	96.5
Avg	**96.8**	**95.7**	**98.5**	**97.7**	**98.8**	**96.7**

Table 1. Dice coefficients (in %) of the lobe-wise evaluation for Experiments 1 and 2: LU = left upper, LL = left lower, RU = right upper, RM = right middle, and RL = right lower lobe. NA = result of the new segmentation approach, whereas PA = the result of the previously published method. Intra1/2 and Inter1/2 are the intra- and interobserver agreement, where 1 refers to a data set with clearly visible fissures and 2 to a data set with incomplete fissures.

3. EXPERIMENTS AND RESULTS

The segmentation method was evaluated on 42 clinical CT datasets, including 16 emphysema, 3 fibrosis, and 12 tumor cases. The in-plane image resolution was between 0.4 mm and 0.8 mm, and the slice thickness was between 0.5 mm and 1.5 mm. Six datasets were low-dose scans. The results were compared with a reference segmentation created by a human expert who manually delineated fissures on 8-15 slices for each lung in each dataset. Subsequently, a deformable surface automatically interpolated the fissures to all in-between slices. With additional interaction, it was possible to modify the segmentation until the desired accuracy was obtained.

In Experiment 1, for each of the 42 data sets, the lobewise Dice coefficient between automatic and reference segmentation was calculated. The average Dice agreement over all data sets is given in Table 1. The same evaluation was performed with the previously published segmentation method [4] to estimate the improvement of the new approach, and thus, the effect of fissure consideration. A paired t-test confirmed the improved performance with a significance of $p < 0.005$. To estimate the reliability of the interactive segmentation, the intra- and interobserver agreement was evaluated in Experiment 2. One data set with clearly visible fissures and one with incomplete fissures were chosen, and Dice coefficients were calculated (Table 1).

4. DISCUSSION AND CONCLUSION

Experiment 1 shows consistent improvement of the segmentation accuracy over the previously published approach [4] (see Table 1). First, the consideration of the fissures decreases inaccuracies at the lobe boundaries. These improvements only slightly influence the Dice coefficient due to the small difference in volume compared to the volume of an entire lobe. Nonetheless, the accuracy at the fissures is particularly important to increase clinical acceptance. Second, the direct enhancement of the fissures in the cost image of the watershed

Authorized licensed use limited to: UCLA Library. Downloaded on August 24,2021 at 19:29:47 UTC from IEEE Xplore. Restrictions apply.

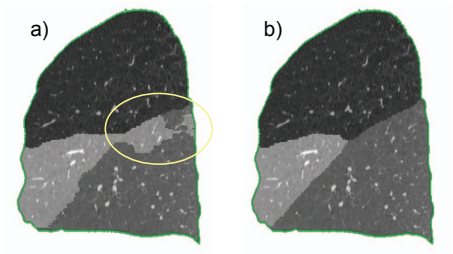

Fig. 5. An exemplary sagittal CT slice showing the results of a) the previously published method with occurring leakage and b) the new approach without leakage.

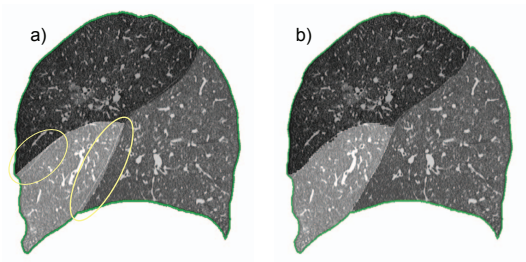

Fig. 6. An exemplary sagittal CT slice showing the results of a) the reference segmentation and b) the automatic segmentation. Note that although the reference segmentation is a good approximation, it is not entirely accurate at the lobar fissures.

can prevent leakage, which was a problem of the former segmentation approach (see Figure 5). The lowest agreement is obtained for the middle lobe, because the minor fissure between upper and middle lobe is often incomplete. In addition, the middle lobe has the smallest volume, so that differences have a stronger effect on the Dice coefficient.

A problem of the quantitative evaluation is the absence of a exact ground truth. Manually tracing the fissures on all CT slices is not feasible if a significant number of data sets is to be evaluated. Rikxoort et al. manually delineated the fissures on every fourth coronal slice for 10 data sets with clearly visible fissures[1] to obtain a reference. Because a complete lobe segmentation is needed to compute volumetric agreement, the decision was made in this work to combine manual tracing with user-verified interpolation. The drawback of this approach is that the interpolated slices are not always entirely accurate, and that the automatic segmentation sometimes appears to be more appropriate than the so-called reference segmentation (see Figure 6).

Experiment 2 analyzes the intra- and interobserver agreement for the reference segmentation on two datasets (see Table 1). As expected, the agreement for the dataset with incomplete fissures was lower than for the data set with clearly visible fissures for both the intra- and the interobserver analysis. This indicates that the quality of the reference segmentation is not only impaired by the interpolation, but also depends strongly on the visibility of the fissures in the data.

The consideration of the pulmonary fissures presented here improves the segmentation accuracy even for pathologic cases. However, the quality of lobe segmentation depends on a good bronchi and vessel tree segmentation. A subject for future work is a weighting of the inputs for the cost image calculation based on the respective segmentation quality. Thus, an inferior segmented bronchi or vessel tree will not compromise the quality of the watershed cost image and the resulting segmentation.

5. REFERENCES

[1] E.M. van Rikxoort, M. Prokop, B. de Hoop, M.A. Viergever, J.P.W. Pluim, and B. van Ginneken, "Automatic segmentation of the pulmonary lobes from fissures, airways, and lung borders: evaluation of robustness against missing data," in *MICCAI*, 2009, pp. 263–271.

[2] L. Zhang, E. A. Hoffman, and J. M. Reinhardt, "Atlas-driven lung lobe segmentation in volumetric X-ray CT images," *IEEE Trans Med Imaging*, vol. 25, no. 1, pp. 1–16, 2006.

[3] E. M. van Rikxoort, B. de Hoop, S. van de Vorst, M. Prokop, and B. van Ginneken, "Automatic segmentation of pulmonary segments from volumetric chest CT scans.," *IEEE Trans Med Imaging*, vol. 28, no. 4, pp. 621–630, 2009.

[4] J.-M. Kuhnigk, V. Dicken, S. Zidowitz, L. Bornemann, B. Kuemmerlen, S. Krass, H.-O. Peitgen, S. Yuval, H.-H. Jend, W. S. Rau, and T. Achenbach, "New tools for computer assistance in thoracic CT – part I: Functional analysis of lungs, lung lobes, and bronchopulmonary segments," *RadioGraphics*, vol. 25, no. 2, pp. 525–536, 2005.

[5] S. Ukil and J. M. Reinhardt, "Anatomy-guided lung lobe segmentation in x-ray CT images.," *IEEE Trans Med Imaging*, vol. 28, no. 2, pp. 202–214, 2009.

[6] J. C. Ross, R. San Jose Estepar, A. Díaz, C.-F. Westin, R. Kikinis, E. K. Silverman, and G. R. Washko, "Lung extraction, lobe segmentation and hierarchical region assessment for quantitative analysis on high resolution computed tomography images," in *MICCAI*, 2009, pp. 690–698.

[7] J. Wang, M. Betke, and J. P. Ko, "Pulmonary fissure segmentation on CT," *Medical Image Analysis*, vol. 10, no. 4, pp. 530 – 547, 2006.

[8] N. Sverzellati, E. Calabro, G. Randi, C. La Vecchia, A. Marchiano, J-M. Kuhnigk, M. Zompatori, P. Spagnolo, and U. Pastorino, "Sex differences in emphysema phenotype in smokers without airflow obstruction," *Eur Respir J*, vol. 33, no. 6, pp. 1320–1328, 2009.

Authorized licensed use limited to: UCLA Library. Downloaded on August 24,2021 at 19:29:47 UTC from IEEE Xplore. Restrictions apply.